Cubic Aluminum Silicides $RE_8Ru_{12}Al_{49}Si_9(Al_xSi_{12-x})$ (RE = Pr, Sm) from Liquid Aluminum. Empty $(Si,Al)_{12}$ Cuboctahedral Clusters and Assignment of the Al/Si Distribution with Neutron Diffraction

B. Sieve,[†] X. Z. Chen,[†] R. Henning,[‡] P. Brazis,[§] C. R. Kannewurf,[§] J. A. Cowen,[⊥,#] A. J. Schultz,[‡] and M. G. Kanatzidis*,[†]

Contribution from the Department of Chemistry, Center for Fundamental Materials Research, and Department of Physics, Michigan State University, East Lansing, Michigan 48824-1322, Argonne National Laboratory, IPNS, Building 360, Argonne, Illinois 60439-4814, and Department of Electrical Engineering and Computer Science, Northwestern University, Evanston, Illinois 60208

Received January 17, 2001

Abstract: Two new quaternary aluminum silicides, $RE_8Ru_{12}Al_{49}Si_9(Al_xSi_{12-x})$ ($x \sim 4$; RE = Pr, Sm), have been synthesized from Sm (or Sm_2O_3), Pr, Ru, and Si in molten aluminum between 800 and 1000 °C in sealed fused silica tubes. Both compounds form black shiny crystals that are stable in air and NaOH. The Nd analog is also stable. The compounds crystallize in a new structural type. The structure, determined by single-crystal X-ray diffraction, is cubic, space group $Pm\bar{3}m$ with $Z = 1$, and has lattice parameters of $a = 11.510(1)$ Å for $Sm_8Ru_{12}Al_{49}Si_9(Al_xSi_{12-x})$ and $a = 11.553(2)$ Å for $Pr_8Ru_{12}Al_{49}Si_9(Al_xSi_{12-x})$ ($x \sim 4$). The structure consists of octahedral units of $AlSi_6$, at the cell center, $Si_2Ru_4Al_8$ clusters, at each face center, $SiAl_8$ cubes, at the middle of the cell edges, and unique $(Al,Si)_{12}$ cuboctohedral clusters, at the cell corners. These different structural units are connected to each other either by shared atoms, Al−Al bonds, or Al−Ru bonds. The rare earth metal atoms fill the space between various structural units. The Al/Si distribution was verified by single-crystal neutron diffraction studies conducted on $Pr_8Ru_{12}Al_{49}Si_9(Al_xSi_{12-x})$. $Sm_8Ru_{12}Al_{49}Si_9(Al_xSi_{12-x})$ and $Pr_8Ru_{12}Al_{49}Si_9(Al_xSi_{12-x})$ show ferromagnetic ordering at $T_c \sim 10$ and ~ 20 K, respectively. A charge of 3+ can be assigned to the rare earth atoms while the Ru atoms are diamagnetic.

Introduction

Transition metal silicides are well-known as both refractory materials and electronic materials. The former are characterized by high hardness, good chemical stability, and high melting points.[1] Transition metal silicides find applications as Si-compatible electrodes for electronics,[2] thermoelectric energy conversion,[3] and infrared detectors[1] among other uses.[4−7] Although binary silicides have been well studied, the ternary and multinary systems are much less extensively studied due to the complexity of multiphase formation and the difficulty of single crystal growth. Silicides are usually synthesized by direct reaction of the elements in a vacuum or in an inert atmosphere; this normally requires reaction temperatures over 1400 °C, mandating the use of an arc-welder or induction furnace. Although annealing or quenching can sometimes yield single crystals, powder samples are usually obtained from these traditional methods. Other preparative methods exist for silicides such as electrochemical synthesis[8] and chemical vapor-deposition[9] but are scarcely used. While metal flux methods have not generally been applied in the synthesis of silicides, sporadic reports do exist. Examples include the lead-flux growth of YCr_2Si_2[10] and the zinc-flux growth of $YbZn_2Si_2$.[11]

Aluminum containing multinary intermetallics are also important phases found in many advanced structural alloys such as aluminum matrix composites.[12] These systems contain a large variety of elements including silicon and form ternary and quaternary compounds within the Al matrix either during preparation or over time. These phases are mainly responsible for the beneficial properties of these alloys but they can also be critical in many failure mechanisms in certain cases. Therefore, detailed knowledge of the chemistry and phase

* To whom correspondence should be addressed.
[†] Department of Chemistry and Center for Fundamental Materials Research, Michigan State University.
[‡] Argonne National Laboratory.
[§] Northwestern University.
[⊥] Department of Physics and Center for Fundamental Materials Research, Michigan State University.
[#] Deceased.

(1) Shah, D. M.; Berczik, D.; Anton, D. L.; Hecht, R. *Mater. Sci. Eng., A* **1992**, *155*, 45−57.
(2) (a) Maex, K. *Mater. Sci. Eng., R* **1993**, *11*, 53−153. (b) Murarka, S. P. *Silicides for VLSI Applications*; Academic Press: New York, 1983, and references therein.
(3) *CRC Handbook of Thermoelectrics*; Rowe, D. M., Ed.; CRC Press: Boca Raton, FL, 1995.
(4) Aronsson, B.; Lundström, T.; Rundqvist, S. *Borides, Silicides and Phosphides*; Methuen & Co. Ltd.: London, 1965.
(5) (a) Schlesinger, M. E. *Chem. Rev.* **1990**, *90*, 607−628. (b) Chart, T. G. *A Critical Assessment of Thermochemical Data for Transition Metal−Silicon Systems*; NPL report on Chemistry 18; National Physical Laboratory: Teddington, U.K., 1972.
(6) Reader, A. H.; Vanommen, A. H.; Weijs, P. J. W.; Wolters, R. A. M.; Oostra, D. J. *Rep. Prog. Phys.* **1993**, *56*, 1397−1467.
(7) Maex, K. *Appl. Surf. Sci.* **1991**, *53*, 328−337.
(8) Shapoval, V. I.; Malyshev, V. V.; Novoselova, I. A.; Kushkhov, K. B. *Russ. Appl. Chem.* **1994**, *67*, 828−833.
(9) Madar, R.; Thomas, N.; Bernard, C. *Mater. Sci. Eng., B* **1993**, *17*, 118−125 and references therein.
(10) Okada S.; Kudou K.; Miyamoto M.; Hikichi Y.; Lundström T. *Nippon Kagaku Kaishi* **1993**, *5*, 681−684.
(11) Grytsiv, A.; Leithe-Jasper, A.; Flandorfer, H.; Rogl, P.; Hiebl, K.; Godart, C.; Velikanova, T. *J. Alloy. Compd.* **1998**, *266*, 7−12.
(12) Suresh, S.; Mortensen, A.; Needleman, A. *Fundamentals of Metal-Matrix Composites*; Butterworth-Heinemann: Boston, 1993.

10.1021/ja010135k CCC: $20.00
Published on Web 06/26/2001

formation in an aluminum matrix could be important in understanding and further developing aluminum matrix composites.

Recently, we introduced a new synthetic approach for silicides using molten Al as a solvent while using metal oxides or elemental metals as reactants.[13] We find that crystals of various metal aluminum silicides grow in liquid Al below 1000 °C, and we have discovered a large number of members of this class of silicides. Al fluxes have been used in the past to prepare borides[14] at very high temperature (>1400 °C) as well as ternary aluminides in the absence of Si or B.[15] Because molten Al dissolves Si without forming a binary compound[16] it is a convenient solvent for the delivery of reactive Si atoms in a reaction system. This approach has already been shown to work well when using first row transition metals. In fact, those compounds with transition metals are particularly attractive since they constitute a separate and interesting class in which the transition metals find themselves in the curious situation where in fact they are the most electronegative atoms in the structure. These circumstances are likely to lead to unusual behavior. From a chemical point of view there are some interesting issues that may arise when considering aluminum intermetallic compounds with transition metals. These include magnetism, structural stability and first-row/second-row similarities. The structural type varies strikingly as one moves across the first row of transition metals forming novel compounds, such as $Sm_2Ni(Si_{1-x}Ni_x)Al_4Si_6$,[17] $RENiAl_4Ge_2$ (RE = Sm, Tb, Y)[18] $Sm_4Fe_{2+x}Al_{7-x}Si_8$,[19] $LaNi_{1+x}Al_4Si_{2-x}$,[20] and $Sm_5(Cu_{4.26}Si_{3.74})Al_8Si_2$[21] under otherwise similar synthetic conditions. In an attempt to probe whether a second row element such as Ru would produce an isostructural compound to Fe we discovered two quaternary rare earth ruthenium aluminum silicides in a novel structure type. Here we report the synthesis, structure, electrical, and magnetic properties of the novel cubic intermetallic compounds $RE_8Ru_{12}Al_{49}Si_9(Al_xSi_{12-x})$ ($x \sim 4$; RE = Pr, Nd, Sm) that crystallize from liquid aluminum. A surprising fragment in the structure is the $(Al,Si)_{12}$ cuboctahedral cluster that has an analogue only in solid-state boron chemistry (e.g., ZrB_{12}[22]), but even in this case the clusters are rare.

Experimental Section

Synthesis. $Sm_8Ru_{12}Al_{49}Si_9(Al_xSi_{12-x})$ ($x \sim 4$). *Method 1*: Sm_2O_3 (Rhone-Poulenc Inc. 99.99%), Ru (Cerac, −325 mesh, 99.95%), Si (Cerac, −325 mesh, 99.96%), and Al metal (Fisher, 20 mesh granular) were initially mixed in a molar ratio of Sm:Ru:Al:Si = 2:1:40:8 and placed into an alumina container, which was then flame sealed in a fused silica tube under high vacuum (<10^{-4} Torr). The sample was heated to 810 °C, kept at that temperature for 8 days, then cooled to 300 °C in 4 days, and finally cooled to room temperature quickly. This method was later repeated using stoichiometric amounts to yield pure product. *Method 2*: In a N_2-filled drybox, Sm (Alfa Aesar, −40 mesh, 99.9%), Ru, and Si were mixed in stoichiometric molar ratios with excess Al metal and transferred into an alumina tube that was then sealed in a quartz tube as described above. The sample was first heated to 1000 °C for 15 h, then cooled to 860 °C in 10 h, kept at 860 °C for 4 days, and finally cooled to 260 °C in 3 days. In both methods, 5 M aqueous NaOH solution was used to remove excess Al flux from the product. The single crystals used for electrical conductivity, thermopower measurements, and magnetic properties were selected from the product of method 2.

$Pr_8Ru_{12}Al_{49}Si_9(Al_xSi_{12-x})$ ($x \sim 4$). *Method 1*: In a N_2-filled drybox, Pr (Alfa Aesar, 40 mesh, 99.9%), Ru, Si, and Al were mixed in a molar ratio of Pr:Ru:Al:Si = 6.5:10:100:8 and transferred into an alumina tube, which was sealed in a fused silica tube as above. The sample was first heated to 1000 °C for 15 h, then cooled to 860 °C in 10 h, kept at 860 °C for 4 days, and finally cooled to 500 °C in 3 days. 5 M aqueous NaOH solution was then used to remove excess Al flux in the product. *Method 2*: Though method 1 produced many crystals, these were too small for the neutron analysis (see below) and grew together forming polycrystalline ingots. Large single crystals, suitable for neutron diffraction, were obtained with a different heating profile than that used above. The reaction mixture was heated to 1000 °C and maintained there for 15 h, followed by cooling to 500 °C in 96 h, slightly longer than the original elemental synthesis. From this procedure, an impure product was obtained but large single crystals of $Pr_8Ru_{12}Al_{49}Si_9(Al_xSi_{12-x})$ ($x \sim 4$) were present, with the largest ones exhibiting dimensions of about 2 mm per side. The major impurity phase found in this synthesis was large crystals of $PrRu_2Al_{10}$.[23] The samples used for magnetic measurements were selected from the product of method 1.

The purity of the final products was confirmed through comparison of the experimental X-ray diffraction powder patterns of the bulk product to theoretical patterns calculated from the refined single-crystal data. Pure $RE_8Ru_{12}Al_{49}Si_9(Al_xSi_{12-x})$ ($x \sim 4$; RE = Sm, Pr) were obtained with all methods (except method 2 for $Pr_8Ru_{12}Al_{49}Si_9(Al_xSi_{12-x})$ ($x \sim 4$)). The Nd analog was also prepared but was not studied in detail.

EDS Analysis. Quantitative microprobe analysis of the compound was performed with a JEOL JSM-35C scanning electron microscope equipped with a Noran Vantage energy dispersive spectroscopy (EDS) detector. Data were acquired by using an accelerating voltage of 25 kV and 100 s accumulation time. Crystals selected from the different synthetic methods were each measured showing no significant differences in their final elemental ratios. The EDS analysis however consistently yielded low values for Al and Si as seen in the past with other compounds.[17] To compensate for this, a standard was used to derive an appropriate correction factor, which was then used to obtain the Al/Si ratio. These analyses, after calibration and averaging yielded a consistent elemental ratio of "$RE_8Ru_{13}Al_{60}Si_{17}$" for both compounds. Typical uncertainties associated with this technique are ±3−5%.

Single-Crystal X-ray Crystallography. Single-crystal X-ray diffraction data of $RE_8Ru_{12}Al_{49}Si_9(Al_xSi_{12-x})$ (RE = Sm, Pr) were collected at room temperature using a Rigaku 4 circle diffractometer with Mo Kα ($\lambda = 0.71073$ Å) radiation. An empirical absorption correction based on Ψ scans was applied to the data. The structure was solved by direct methods (SHELXS-86[24]) within the TEXSAN[25] crystallographic software package. The structure was then further refined with the SHELXL[26] package of programs. The crystallographic and refinement data are listed in Table 1. The fractional atomic positions, displacement

(13) (a) Chen, X. Z.; Sieve, B.; Henning, R.; Schultz, A. J.; Brazis, P.; Kannewurf, C. R.; Cowen, J. A.; Crosby R.; Kanatzidis, M. G. *Angew. Chem., Int. Ed.* **1999,** *38*, 693−696.

(14) Okada, S.; Yu, Y.; Lundström, T.; Kudou, K.; Tanaka T. *Jpn. J. Appl. Phys*. **1996**, *35*, 4718−4723.

(15) (a) Niemann, S.; Jeitschko, W. *J. Solid State Chem.* **1995**, *114*, 337−341. (b) Niemann, S.; Jeitschko, W. *Z. Kristallogr*. **1995**, *210*, 338−341. (c) Niemann, S.; Jeitschko, W. *J. Solid State Chem*. **1995**, *116*, 131−135. (d) Niemann, S.; Jeitschko, W. *J. Alloys Compd*. **1995**, *221*, 235−239.

(16) *Binary Alloy Phase Diagrams*; Massalski, T. B., Ed.; American Society for Metals: Metals Park, OH, 1986.

(17) Chen, X. Z.; Sportouch, S.; Sieve, B.; Brazis, P.; Kannewurf, C. R.; Cowen, J. A.; Patschke, R.; Kanatzidis, M. G. *Chem. Mater*. **1998**, *10*, 3202−3211.

(18) Sieve, B.; Chen, X. Z.; Cowen, J. A.; Larson, P.; Mahanti, S. D.; Kanatzidis, M. G., *Chem*. *Mater*. **1999**, *11*, 2451−2455.

(19) Sieve, B.; Sportouch, S.; Chen, X. Z.; Cowen, J. A.; Brazis, P.; Kannewurf, C. R.; Papaefthymiou, V.; Kanatzidis, M. G. *Chem. Mater*. **2001**, *13*, 272−283.

(20) Sieve, B.; Kanatzidis, M. G. To be submitted for publication.

(21) Sieve, B.; Chen, X. Z.; Kanatzidis, M. G. Manuscript in preparation.

(22) Kennard, C. H. L.; Davis, L. *J. Solid State Chem*. **1983**, *47*, 103−106.

(23) Thiede, V. M. T.; Ebel, T.; Jeitschko, W. *J. Mater. Chem.* **1998**, *8*, 125−130.

(24) Sheldrick, G. M. In *Crystallographic Computing 3*; Sheldrick, G. M., Kruger, C. C., Doddard, R., Eds.; Oxford University Press: Oxford, UK, 1985; pp 175−189.

(25) *TEXSAN*, TEXRAY Structure Analysis Package; Molecular Structure Corporation: The Woodlands, TX, 1992.

(26) Sheldrick, G. M. *SHELXL*, Structure Determination Programs, Version 5.0; Siemens Analytical X-ray Instruments Inc.: Madison, WI, 1995.

Table 1. Crystallographic Data for $RE_8Ru_{12}Al_{49}Si_9(Al_xSi_{12-x})$ ($x \sim 4$; RE = Sm, Pr)

empirical formula	$Sm_8Ru_{12}Al_{53}Si_{17}$	$Pr_8Ru_{12}Al_{53}Si_{17}$	$Pr_8Ru_{12}Al_{53}Si_{17}$
radiation	Mo Kα ($\lambda = 0.71069$ Å)	Mo Kα	neutron α (λ= 0.7−4.2 Å)
formula weight	4324	4247.7	4247.7
crystal system	Cubic	Cubic	Cubic
space group	$Pm\bar{3}m$ (No. 221)	$Pm\bar{3}m$	$Pm\bar{3}m$
crystal size (mm)	0.10 × 0.14 × 0.30	0.20 × 0.20 × 0.16	1.5 × 1.5 × 2.0
a (Å)	11.510(1)	11.553(2)	11.553(1)
V (Å$^{3)}$	1524.9(3)	1541.9(4)	1541.9(4)
Z	1	1	1
d_{calc} (g cm$^{-3)}$	4.708	4.574	4.574
θ range (deg)	1.77 to 29.98	1.76 to 29.99	NA
diffractometer	Rigaku AFC6S	Rigaku AFC6S	SCD at IPNS
temp (K)	298	298	298
μ (mm^{-1})	11.518	10.094	0.0135 × 0.005·λ
index ranges	$-16 \le h \le 16$	$-16 \le h \le 16$	$-14 \le h \le 7$
	$-11 \le k \le 11$	$-11 \le k \le 11$	$-19 \le k \le 5$
	$-9 \le l \le 9$	$-9 \le l \le 9$	$-5 \le l \le 18$
no. of reflcns collected	3561	3588	1398
no. of unique reflcns	568 [R(int) = 0.031]	511 [R(int) = 0.052]	325
goodness of fit	1.666	1.379	1.96
R indices[a]	$R1 = 0.035$, $wR2 = 0.083$	$R1 = 0.0178$, $wR2 = 0.0402$	$R(F) = 0.086$, $R_w(F) = 0.062$
R indices[a] (all data)	$R1 = 0.045$, $wR2 = 0.124$	$R1 = 0.0282$, $wR2 = 0.1115$	
max peak and hole	1.949 and −2.036 e$^-$/Å^3	0.762 and −0.939 e$^-$/Å^3	

[a] $R1 = \sum||F_o| - |F_c||/\sum|F_o|$, $wR2 = [\sum(|F_o^2 - F_c^2|)^2/\sum(wF_o^2)^2]^{1/2}$, and $I > 2\sigma(I)$ for X-ray data. $R(F) = \sum||F_o| - |F_c||/\sum|F_o|$, $R_w(F) = [\sum(|F_o - F_c|)/\sum(wF_o)]^{1/2}$, and $I > 3\sigma(I)$ for neutron data.

parameters (U values), and selected bond distances and angles are given in the Supporting Information.

As in any Al- and Si-containing compound, these two elements are difficult to distinguish by X-ray diffraction alone due to their similar X-ray scattering cross sections. However, in most cases the assignment can be made on the basis of bond lengths around Al and Si. Our assignment produced reasonable bond distances consistent with those in the literature except for the Si(1)−Al(3) distances of 2.789(3) and 2.828(2) Å for M = Sm and Pr, respectively, in the $AlSi_6$ octahedra (see below structural description) which are also reasonable for Al−Al bonds. The Si(1)−Sm distance (2.9894(9) Å), however, suggests that the assignment of Si is correct since the Al−Sm distance should be slightly longer at 3.25 to 3.32 Å.[22,27] The final X-ray structure gave the lowest R values and the best temperature factors. Nevertheless, ambiguity still remained in this part of the structure so a single crystal neutron diffraction study was used to resolve it since the neutron scattering lengths of aluminum and silicon differ sufficiently to allow accurate identification of each element.[28]

Neutron Diffraction. A single crystal (1.5 × 1.5 × 2 mm^3) of $Pr_8Ru_{12}Al_{49}Si_9(Al_xSi_{12-x})$ was mounted on an aluminum pin and placed on the SCD diffractometer at the Intense Pulsed Neutron Source (IPNS) at Argonne National Laboratory. A position-sensitive area detector was used to obtain time-of-flight Laue diffraction data with a wavelength range of 0.7−4.2 Å at room temperature for 18 settings of the crystal, which covered at least one octant of reciprocal space.[29] The details of the data collection and analysis procedures have been described previously.[30] An autoindexing routine was used to obtain an orientation matrix[31] and integrated intensities were corrected for the Lorentz factor and the incident spectrum. A wavelength-dependent spherical absorption correction was applied[32] but symmetry-related reflections were not averaged because extinction is strongly wavelength dependent. The structural refinement was then performed using the GSAS program.[33]

The initial ordering as determined from the X-ray analysis (taken from Table 2 but with all positions fully occupied) provided a starting model for the neutron data. The only possible indications of error were seen in the thermal parameters for the Si(2) and M(1) positions. The Si(2) position had anisotropic thermal parameters that were slightly larger than expected but still reasonable. The thermal parameters for the M(1) position were strongly distorted with the U_{22} direction close to 0. Attempts to improve the refinement by exchanging Si for Al or vice versa led to unacceptable thermal parameters (negative or extremely large) for each of these six positions confirming the original X-ray assignments. The possibility of mixing both Si and Al on the same site was then explored by allowing all of the fractional occupancies of the Al/Si positions to refine. All positions refined to full occupancy of either Si or Al (within 1 σ) except for the Si(2) and M(1) positions.

Table 2. Atomic Positions and Equivalent Isotropic Displacement Parameters (Å^2) for $RE_8Ru_{12}Al_{49}Si_9(Al_xSi_{12-x})$ ($x \sim 4$; RE = Sm, Pr) in Space Group $Pm\bar{3}m$[a]

atom	position	x	y	z	U(eq)[b]
Sm	8*g*	0.3221(1)	0.3221(1)	0.3221(1)	7(1)
Pr (X-ray)		0.3211(1)	0.3211(1)	0.3211(1)	6(1)
Pr (neutron)		0.3213(2)	0.3213(2)	0.3213(2)	4.8(6)
Ru	12*i*	0.3056(1)	0	0.3056(1)	8(1)
		0.3054(1)	0	0.3054(1)	5(1)
		0.3055(9)	0	0.3055(9)	5.2(6)
M(1)[c]	12*i*	0.1571(2)	0	0.1571(2)	15(1)
		0.1568(1)	0	0.1568(1)	13(1)
		0.1570(2)	0	0.1570(2)	16.1(1)
Si(1)	6*f*	0.5	0.2577(3)	0.5	8(1)
		0.5	0.2552(2)	0.5	6(1)
		0.5	0.2554(4)	0.5	6.7(2)
Si(2)	3*d*	0	0	0.5	9(1)
		0	0	0.5	7(1)
		0	0	0.5	9.1(2)
Al(1)	24*l*	0.5	0.1130(2)	0.3223(1)	9(1)
		0.5	0.1121(1)	0.3216(1)	7(1)
		0.5	0.1122(2)	0.3220(2)	7.2(1)
Al(2)	24*m*	0.1277(1)	0.3618(2)	0.1277(1)	10(1)
		0.1270(1)	0.3615(1)	0.1270(1)	9(1)
		0.1269(1)	0.3611(2)	0.1269(1)	7.67(9)
Al(3)	1*b*	0.5	0.5	0.5	7(1)
		0.5	0.5	0.5	13(1)
		0.5	0.5	0.5	8.6(3)

[a] Note: Each first line is for M = Sm (X-ray). Each second line is for M = Pr (X-ray). Each third line is for Pr (neutron). [b] U(eq) is defined as one-third of the trace of the orthogonalized U_{ij} tensor. [c] In the Neutron refinement the occupancy of this position is refined to 37/63(7) Al/Si. All other positions are fixed to 100% occupancy.

(27) Schäfer, W.; Will, G.; Gal, J.; Suski, *W. J. Less-Common Met.* **1989**, *149*, 237−241.

(28) *International Tables of Crystallography*; Wilson, A. J. C., Ed.; Kluwer Academic Publishers: Dordrecht, The Netherlands, 1995; Vol. C.

(29) Schultz, A. J. *Trans. Am. Crystallogr. Assoc.* **1987**, *23*, 61.

(30) Schultz, A. J.; Srinivasan, K.; Teller, R. G.; Williams, J. M.; Lukehart, C. M. *J. Am. Chem. Soc.* **1984**, *106*, 999.

(31) Jacobson, R. A. *J. Appl. Crystallogr.* **1986**, *19*, 283.

(32) Howard, J. A. K.; Johnson, O.; Schultz, A. J.; Stringer, A. M. *J. Appl. Crystallogr.* **1987**, *20*, 120.

(33) Larson, A. C.; Von Dreele, R. B. *GSAS*, General Structure Analysis System; Los Alamos National Laboratory: Los Alamos, NM, 1994.

The refinement of the Si(2) position suggested approximately 34(15)% occupancy by Al. Since the standard deviation was quite large, however, this position was fixed to be fully occupied by Si in the final refinement. The refinement of the fractional occupancy of the M(1) position yielded an Al/Si occupancy of 37/63(7)% but with a much smaller standard deviation as compared to the Si(2) position. This improved the thermal parameters of the M(1) position although some unusual anisotropy was still observed. Fourier plots of this site did not reveal any splitting and all attempts to model the atoms as disordered over two distinct sites failed. The nonspherical nature of this site was also observed in the X-ray refinement and is currently believed to be an inherent property of this structure.

If no mixing of Al/Si occurs in any position then the final Al:Si ratio would be 6.78:1 for the entire unit cell. If mixing on the M(1) is considered then the Al:Si ratio drops to 3.23, which is in fair agreement with the EDS result of 3.47. Although the Si(2) position was fixed to full occupancy in this refinement, an Al:Si ratio of 3.58 would be obtained if some Al were included in this site. It should also be noted that the samarium analogue yielded a similar Al:Si ratio from EDS measurements which further supports the mixed occupancy disorder model. Data collection parameters, atomic positions, and bond distance and angle information is provided in Tables 1, 2, and 3, respectively.

Electrical and Magnetic Properties. DC electrical conductivity and thermopower measurements were completed on selected single crystals. Conductivity measurements were performed with the conventional four-probe technique.[34] Thermopower measurements were made using a slow AC technique as described elsewhere.[35]

Magnetic susceptibility for $RE_8Ru_{12}Al_{49}Si_9(Al_xSi_{12-x})$ ($x \sim 4$; RE = Sm, Pr) was measured as a function of both temperature and field using a MPMS Quantum Design SQUID magnetometer. An initial study of field dependence was conducted to find a field suitable for the temperature-dependence studies. Temperature-dependence measurements on polycrystalline samples were then conducted under increasing temperature within a 500 G field. Field-dependent measurements were conducted at 5 K in fields between ±55 000 G.

Results and Discussion

Synthesis with Liquid Aluminum. Molten aluminum is an excellent medium for the synthesis of multinary aluminum containing silicides. The combination of rare earth elements, transition metals, and silicon in excess liquid Al conveniently gives large crystals of ternary and quaternary compounds, often exhibiting interesting new structural arrangements. Due to the eutectic nature of the Si/Al interaction[16] a large amount of Si can be dissolved while remaining highly reactive in liquid Al. The presence of dissolved Si creates excellent reaction conditions with other elements, even if they are only present in small percentages or are only partially dissolved. In this work, both compounds were grown as well formed shiny black crystals with a cuboctahedral shape, see Figure 1. The compounds are stable in air, water, and aqueous NaOH solution; however, they decompose instantaneously in dilute aqueous HCl.

The Al flux also permits the use of metal oxide starting materials which decreases costs and allows reactant handling in ambient atmosphere. When a metal oxide precursor is used, the Al acts as a reducing agent converting the metal oxides into dispersed fine particles of reactive metal. The reaction temperature can then be lower since the metals formed in situ are more reactive. A powerful force in the process is the formation of Al_2O_3, which drives this reduction in a manner reminiscent of the thermite reaction.[36] Therefore, larger quantities of Al are recommended to compensate for the formation of Al_2O_3.

(34) Lyding, J. W.; Marcy, H. O.; Marks, T. J.; Kannewurf, C. R. *IEEE Trans. Meas.* **1988**, *37*, 76−80.
(35) Marcy, H. O.; Marks, T. J.; Kannewurf, C. R. *IEEE Trans Instrum. Meas.* **1990**, *39*, 756−760.
(36) Nebergall, W.; Schmidt, F.; Holtzclaw, H., Jr. *General Chemistry*; D. C. Health and Company: Lexington, 1972; p 845.

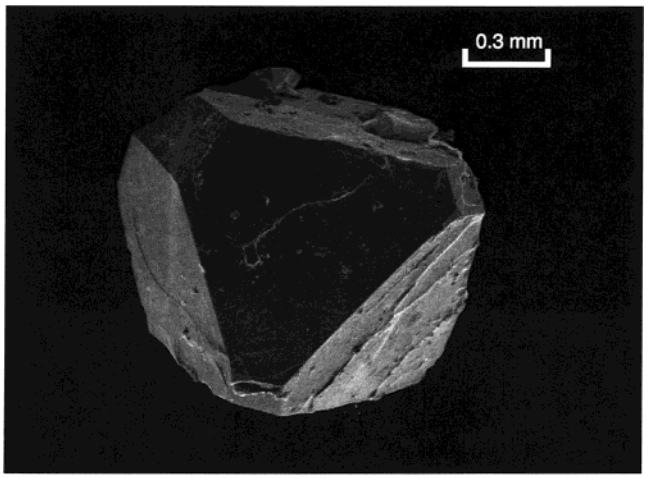

Figure 1. SEM image of a crystal of $Pr_8Ru_{12}Al_{49}Si_9(Al_xSi_{12-x})$ with typical morphology.

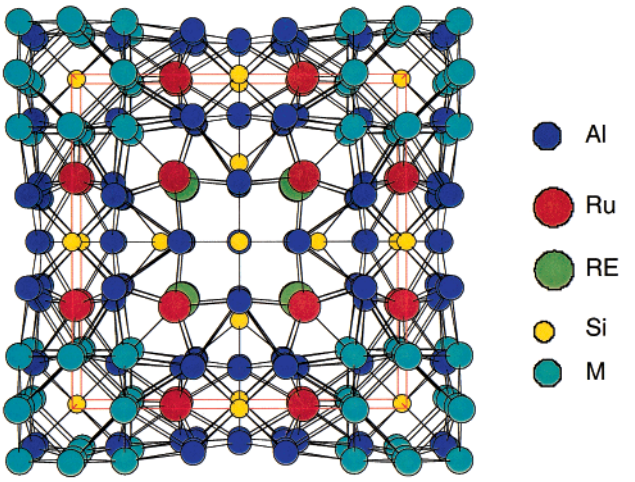

Figure 2. Structure of $RE_8Ru_{12}Al_{49}Si_9(Al_xSi_{12-x})$ (RE = Pr, Sm) (one unit cell shown).

Structure Description. The compounds $RE_8Ru_{12}Al_{49}Si_9(Al_xSi_{12-x})$ ($x \sim 4$; RE = Pr, Sm) adopt a new, rather elaborate structure type with $Pm\bar{3}m$ symmetry, see Figure 2. Because the corresponding distances in both compounds are similar only those in the Sm analogue will be mentioned, unless specifically indicated. This complex three-dimensional assembly of atoms can be more easily understood, if it is conceptually separated into different parts based on the structural features and location in the cell. These include an octahedron $AlSi_6$ at the cell center, $Si_2Ru_4Al_8$ clusters at each face center, $SiAl_8$ cubes at the middle of the cell edges, and (Al_xSi_{12-x}) clusters at the cell corners. Each of these individual building blocks and their position in the unit cell are shown in Figure 3.

The $AlSi_6$ octahedron, at the cell center, contains an Al(3) atom that is coordinated by six Si(1) atoms at distances of 2.789(3) Å (see Figures 3A and 4). The $AlSi_6$ octahedron is ideal and shares its six corners with six $Si_2Ru_4Al_8$ clusters, which are located at the face center position of the cubic cell, Figure 4. The $Si_2Ru_4Al_8$ cluster consists of an aluminum square prism capped with four Ru and two Si(1) atoms, Figure 3B. While the Al(1)−Al(1) bond distances are 2.601(4) Å in $Sm_8Ru_{12}Al_{49}Si_9(Al_xSi_{12-x})$ ($x \sim 4$), the Ru−Al(1) and Si(1)−Al(1) bond distances are 2.596(1) and 2.638(3) Å. This type of moiety has been seen in several other compounds recently discovered, using molten Al as a flux, as a merged unit forming $NiAl_4Si_2$ layers.[17] However, in the previous compounds the unit is fused with other

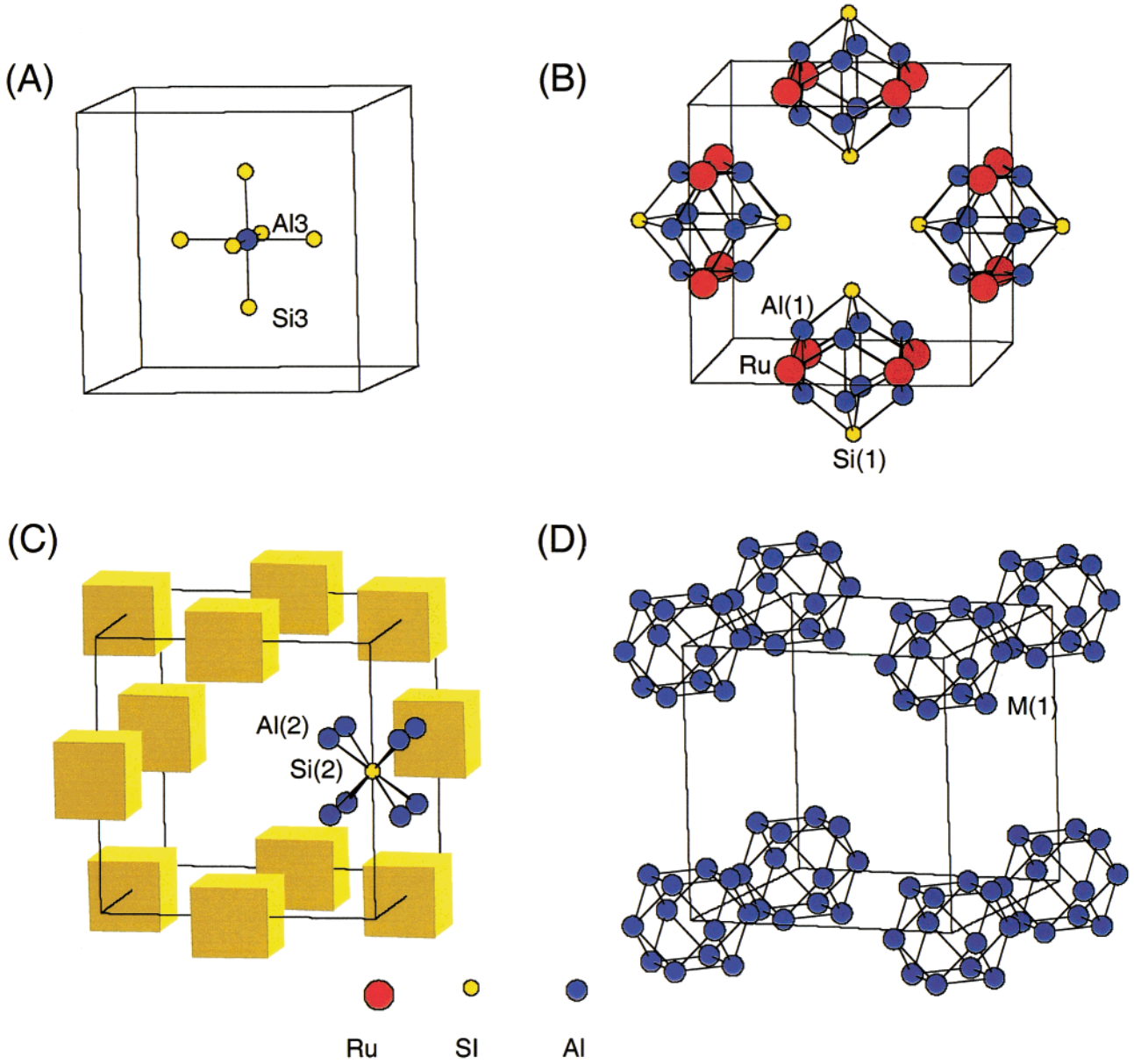

Figure 3. Structural units of $RE_8Ru_{12}Al_{49}Si_9(Al_xSi_{12-x})$ ($x \sim 4$; RE = Pr, Sm): (A) $AlSi_6$ unit at the body center position, (B) $Ru_2Al_8Si_2$ units found at the center of cell faces (two units of $Ru_2Al_8Si_2$ were removed for clarity), (C) $SiAl_8$ units at the center of cell edges, and (D) the (Al_xSi_{12-x}) ($x \sim 4$) units at the cell corners.

such units by sharing faces to form slabs and consequently is hard to recognize. In $RE_8Ru_{12}Al_{49}Si_9(Al_xSi_{12-x})$ it is found as a discrete cluster. While sharing Si sites with two separate $AlSi_6$ octahedra along one axis, the $Si_2Ru_4Al_8$ cluster also connects, along the perpendicular plane, four $SiAl_8$ cubes comprised of Si(2) and eight Al(2) atoms, which occupy the middle of each of the 12 cell edges, Figure 3C. The $SiAl_8$ cube and the $Si_2Ru_4Al_8$ cluster bonding is facilitated by Al(2)−Al(1) and Al(2)−Ru bonds, see Figure 5A.

The $SiAl_8$ units also link to two M_{12} (Al_xSi_{12-x}) clusters along the *a*-axis, Figure 5B. The M_{12} clusters comprised of the mixed Al/Si site (see the neutron refinement section above), are located at the corners of the cubic cell to complete the basic three-dimensional structure. The M(1)−M(1) bond distances in the M_{12} cluster are 2.557(3) Å for $Sm_8Ru_{12}Al_{49}Si_9(Al_xSi_{12-x})$.

The M_{12} type of arrangement is found in $LiAl_3$,[37] where Li atoms are surrounded by 12 Al atoms in a cuboctahedral geometry. However, we note that there are no discernible cuboctahedral Al_{12} clusters in $LiAl_3$. The inside diameter is 5.671 Å with Li−Al and Al−Al bond distances of 2.836(3) Å. The M_{12} unit in $RE_8Ru_{12}Al_{49}Si_9(Al_xSi_{12-x})$ has an inside diameter of 5.114 Å (RE = Sm), which appears too small to allow interstitial atoms inside. The considerably shorter M−M bonds of 2.56 Å in M_{12} compared to those in $LiAl_3$ are consistent with the substantial occupation of the M(1) site with silicon. A boron analogue exists in the form of the B_{12} cubooctahedron in ZrB_{12}. The B_{12} cluster found in AlB_{12}[38] is different as it exhibits an icosahedral geometry. The (Al_xSi_{12-x}) clusters in $RE_8Ru_{12}Al_{49}Si_9(Al_xSi_{12-x})$ are easily recognized because they are enveloped in a cavity of Ru atoms, see Figure 6. The Ru−M bond distance is 2.416(3) Å (in Sm analog). Other important distances associated with this fragment are given in Table 3.

The rare earth atoms occupy the space between the building units described above in a 12-coordinate bonding arrangement

(37) Yoshiyama, T.; Hasebe, K.; Mannami, M.-H. *J. Phys. Soc. Jpn.* **1968**, *25*, 908.
(38) Higashi, I.; Sakurai, T.; Atoda. T. *J. Solid State Chem.* **1977**, *20*, 67−77.

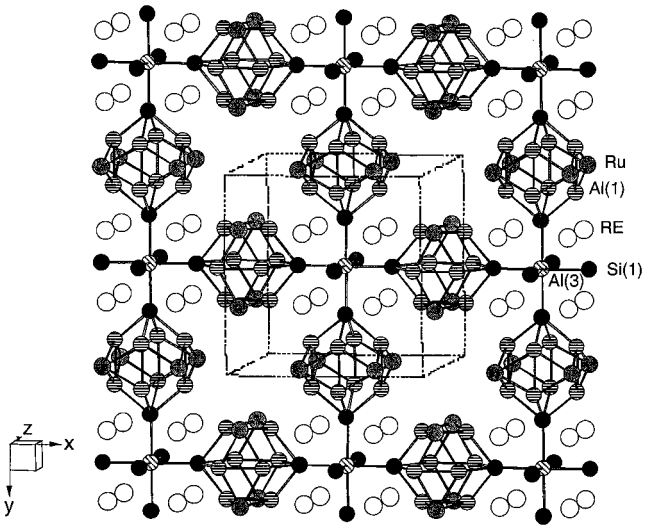

Figure 4. View of the $AlSi_6$ octahedron at the cell center sharing Si atoms with the $Ru_2Al_8Si_2$ clusters at the face centers.

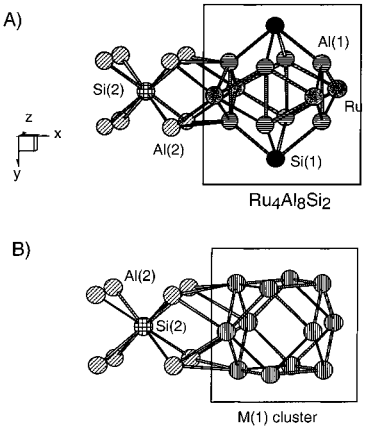

Figure 5. (A) The $SiAl_8$ cube and the $Ru_4Al_8Si_2$ clusters bonding through Al−Al and Al−Ru bonds (B) and a $SiAl_8$ cube linked to a M_{12} cluster through Al−Al bonds.

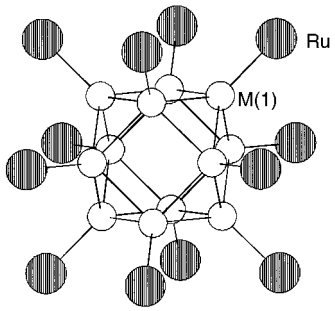

Figure 6. The cuboctahedral (Al_xSi_{12-x}) cluster surrounded by a "coating" of Ru atoms shown to 2.5 Å from the M atom.

of a distorted anticuboctahedron,[39] Figure 7A. The Ru atoms in the structure are surrounded by nine atoms in a distorted monocapped cube arrangement, bonding to four Al(1) atoms, four Al(2) atoms, and an M(1) atom, Figure 7B. Si(1) exhibits a square pyramidal environment (omitting bonds to RE) and bonding to four Al(1) atoms and an Al(3) atom (Figure 7C), while Si(2) exhibits as a cube bonding to eight Al(2) atoms (Figures 3C). The mixed Al/Si disorder position M(1) exhibits a monocapped cube arrangement seen in Figure 7D.

(39) Parthe, E. *Elements of Inorganic Structural Chemistry*; K. Sutter Parthe: Switzerland, 1996; p 15.

Table 3. Selected Bond Distances (Å) and Angles (deg) for $RE_8Ru_{12}Al_{49}Si_9(Al_xSi_{12-x})$ ($x \sim 4$; RE = Sm, Pr) Bond Distances (Å)

	M = Sm	M = Pr (X-ray)	M = Pr (neutron)
RE−Si(1)	2.9894(9)	3.0206(8)	3.018(2)
RE−Al(1)	3.160(2)	3.178(1)	3.177(2)
RE−Al(2)	3.197(2)	3.206(1)	3.209(3)
Ru−Al(1)	2.596(1)	2.6010(8)	2.602(2)
Ru−Al(2)	2.6021(6)	2.6120(6)	2.611(1)
Ru-M(1)	2.416(3)	2.429(2)	2.426(4)
Si(1)−Al(1)	2.638(3)	2.642(2)	2.639(4)
Si(1)−Al(3)	2.789(3)	2.828(2)	2.826(4)
Si(2)−Al(2)	2.617(2)	2.620(1)	2.622(2)
Al(1)−Al(1)	2.601(4)	2.591(2)	2.593(5)
Al(1)−Al(2)	2.752(2)	2.765(2)	2.772(3)
Al(2)-M(1)	2.798(2)	2.805(2)	2.798(3)
M(1)-M(1)	2.557(3)	2.561(2)	2.565(4)

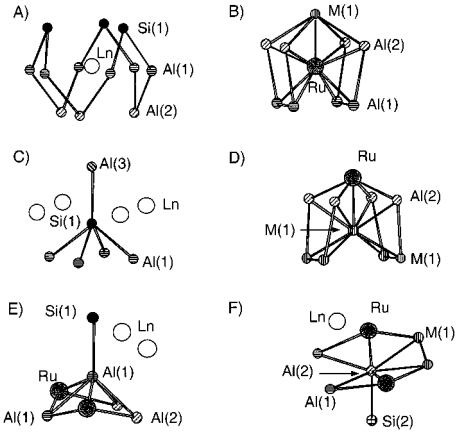

Figure 7. Local coordination environments of the various atoms in the unit cell of $RE_8Ru_{12}Al_{49}Si_9(Al_xSi_{12-x})$, with labeling.

The pure Al positions in the structure exhibit environments varying from a simple octahedron to a highly distorted bicapped trigonal pyramidal arrangement. Al(1) exhibits the distorted bicapped trigonal pyramidal environment shown in Figure 7E, with bonding to two Ru atoms, two Al(2) atoms, an Al(1) atom, and a Si(1) atom. The Al(2) environment, Figure 7F, has a similar arrangement bonding to two Ru atoms, two Al(1) atoms, two M(1) atoms, and a Si(2) atom. At a distance of 2.940 Å from Al(2) we find two additional Al(2) atoms which are not shown in the figure. Finally Al(3) exhibits octahedral bonding to six Si(1) atoms, see Figures 3A.

Charge Transport Properties. Electrical conductivity measurements on single crystals of $Sm_8Ru_{12}Al_{49}Si_9(Al_xSi_{12-x})$ show metallic properties with a moderate room temperature value of about 4000 S/cm at room temperature, see Figure 8A, which rises as the temperature decreases. This behavior is in agreement with the metallic character shown by the thermopower measurements.

Thermopower measurements on single crystals of $Sm_8Ru_{12}Al_{49}Si_9(Al_xSi_{12-x})$ were carried out over a temperature range of 50−300 K while the electrical conductivity measurements were conducted between 5 and 300 K. The thermopower values are small, with a value of about $-4\ \mu$V/K at room temperature (see Figure 8B), which is indicative of the expected metallic behavior of these compounds. The decrease in thermopower as the temperature approaches zero is consistent with this expectation.

Magnetic Properties. $Sm_8Ru_{12}Al_{49}Si_9(Al_xSi_{12-x})$ ($x \sim 4$) exhibits a ferromagnetic transition with T_c of 10 K, Figure 9A, and does not follow Curie−Weiss behavior. This is typical for

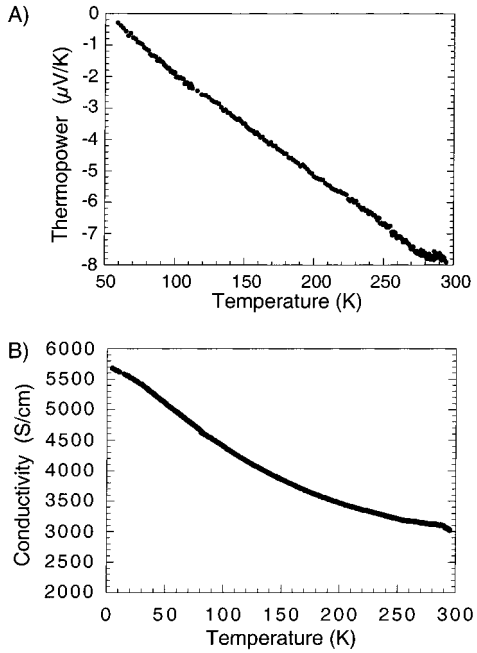

Figure 8. (A) Thermopower of a single crystal of $Sm_8Ru_{12}Al_{49}Si_9(Al_xSi_{12-x})$ ($x \sim 4$). Values shown have been corrected for the contribution of the Au electrodes used to make contacts to the samples. (B) Electrical conductivity data from a single crystal of $Sm_8Ru_{12}Al_{49}Si_9(Al_xSi_{12-x})$ as a function of temperature.

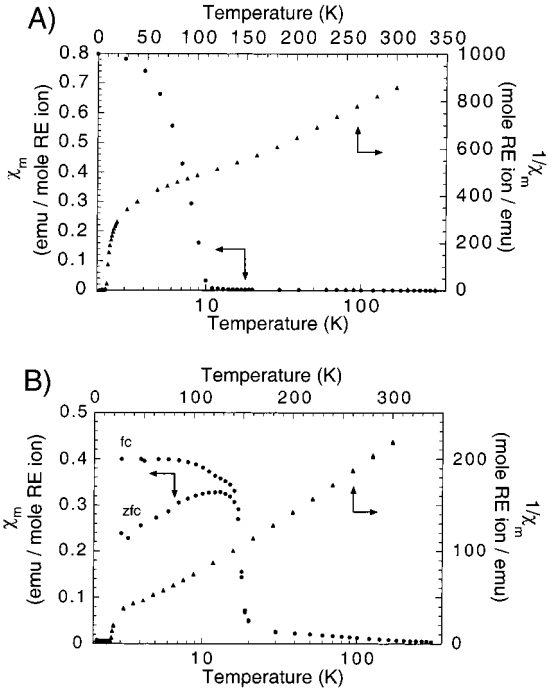

Figure 9. Magnetic susceptibility vs temperature for (A) $Sm_8Ru_{12}Al_{49}Si_9(Al_xSi_{12-x})$. The data do not follow Curie−Weiss behavior <150 K. (B) $Pr_8Ru_{12}Al_{49}Si_9(Al_xSi_{12-x})$, applied field 500 G.

many Sm^{3+} systems (f^6 configuration) where the spacing of the multiplet energy levels above the ground state is small compared to kT causing thermal population of excited magnetic states.[40] The Pr analogue also exhibits a ferromagnetic transition with T_c of 20 K but it does follow Curie−Weiss behavior above 30 K with a Weiss constant θ of 8 K, Figure 9B. From the data a μ_{eff} of 3.40(1) B.M. can be obtained per Pr atom, which is very

(40) Bourdreaux, E. A.; Mulay, L. N. In *Theory and Applications of Molecular Paramagnetism*; John Wiley and Sons: New York, 1976.

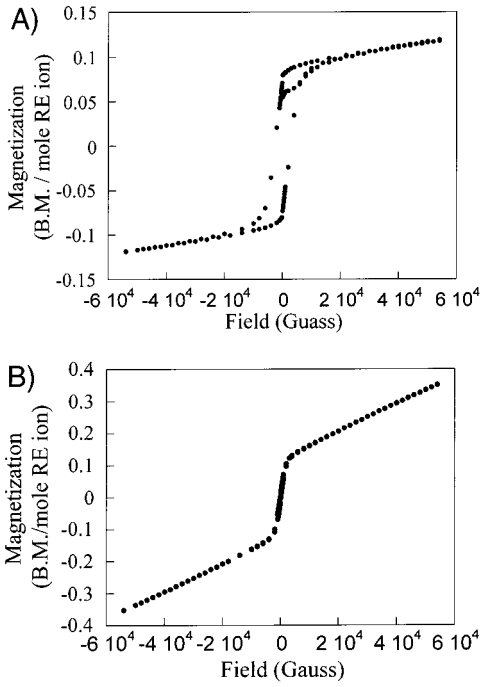

Figure 10. The magnetization vs field curves for (A) $Sm_8Ru_{12}Al_{49}Si_9(Al_xSi_{12-x})$ and (B) $Pr_8Ru_{12}Al_{49}Si_9(Al_xSi_{12-x})$ at 5 K.

close to the theoretical value of 3.58(1) B.M. for a Pr^{3+} ion.[39] The good agreement suggests diamagnetic behavior for all other atoms in the structure, highlighting the absence of magnetic moment on the Ru atoms. This appears to be a common feature of many aluminum-rich intermetallics containing transition metals. For example, similar lack of transition metal magnetism was observed in $Sm_4Fe_{2+x}Al_{7-x}Si_8$,[19] $Sm_2Ni(Si_{1-x}Ni_x)Al_4Si_6$,[17] $LaNi_{1+x}Al_4Si_{2-x}$, $ReFe_2Al_{10}$, and $RERu_2Al_{10}$[22] and arises from a complete filling of the d-orbital manifold and strong hybridization with the surrounding Al and Si orbitals.

The diamagnetism of Ru can also be understood if we consider that it is one of the most electronegative elements in the structure (2.2 Pauling scale), even more so than Si (1.8). At least based on electronegativity arguments, electrons in the structure should flow from Sm and Al[41] to Ru filling the d-orbital shell. This is very much in accord with the results of extended Hückel band structure calculations, which show that the Ru d orbitals are concentrated in a very narrow set of bands that are completely filled and substantially energetically stabilized (∼5 eV below the Fermi level).[42] It is also in agreement with other calculations on intermetallic compounds which suggest similar behavior.[17]

The magnetization vs field curve at 5 K for the Sm compound exhibits a hysteresis with a coercive field of approximently 6500 G, Figure 10A. The nonreversibility between increasing and decreasing fields is evident until 5000 G when the curves merge. The magnetization then continues to increase slowly with field out to the maximum measured value of 55 000 G with no sign of full magnetic saturation. The field-dependent magnetization of $Pr_8Ru_{12}Al_{49}Si_9(Al_xSi_{12-x})$, Figure 10B, exhibits a change in slope at 2000 G but no significant coercive field. After the change in slope the magnetization increases linearly as a function of field, as seen in the Sm analogue, with no sign of magnetic saturation.

(41) Of course, electron−electron interaction and exchange interactions could affect this hypothesis or at least render it more qualitative.

(42) Sieve, B.; Sportouch, S. P.; Kanatzidis, M. G. Unpublished results.

Concluding Remarks

Liquid Al is a convenient and effective medium for exploratory synthesis of intermetallic aluminum silicides. The ferromagnetic cubic compounds, $RE_8Ru_{12}Al_{49}Si_9(Al_xSi_{12-x})$ ($x \sim 4$; RE = Pr, Nd, Sm) form in aluminum solutions containing Sm, Sm_2O_3 or Pr, Ru, and Si between 1000 and 800 °C in sealed silica tubes. The three-dimensional structure includes the notable cuboctahedral $(Al_xSi_{12-x})_{12}$ clusters. The RE atoms are in a 3+ oxidation state while the Ru atoms are diamagnetic. The dramatic difference observed between the chemistry of Fe and Ru in these intermetallic systems is particularly noteworthy as can be seen from the different phases obtained for $RE_4Fe_{2+x}Al_{7-x}Si_8$ (RE = Ce, Pr, Nd, Sm) and $RE_8Ru_{12}Al_{49}Si_9(Al_xSi_{12-x})$ (RE = Pr, Nd, Sm). In both systems, however, the absence of magnetic moment on the transition metal suggests that this is a recurring theme in this chemistry in which the transition metals (unlike in more conventional compounds) are now the most electronegative species in the structure. The recognition that the later transition metals can in fact act as electron acceptors in aluminum intermetallics is revealing and can lead to new avenues of experimentation that may not otherwise have been followed. It would be interesting to determine how far to the left in the transition series we have to go to observe a change in this behavior.

Acknowledgment. Financial support from the Department of Energy (Grant No. DE-FG02-99ER45793) is gratefully acknowledged. This work made use of the SEM facilities of the Center for Electron Optics at Michigan State University. We would like to thank Professor Gordie J. Miller for fruitful discussions.

Supporting Information Available: Tables of crystal data and structure refinement details, atomic coordinates, anisotropic displacement parameters of all atoms, and bond angles and distances for the structure (PDF). This material is available free of charge via the Internet at http://pubs.acs.org.

JA010135K